



**AIAA 97-0060**

**Decay Characteristics of Wake Vortices from Jet  
Transport Aircraft**

J.N. Hallock

Volpe National Transportation Systems Center  
Cambridge, MA

D.C. Burnham

Scientific & Engineering Solutions, Inc.  
Orleans, MA

**35th Aerospace Sciences  
Meeting & Exhibit**  
January 6-10, 1997 / Reno, NV

# DECAY CHARACTERISTICS OF WAKE VORTICES FROM JET TRANSPORT AIRCRAFT

J. N. Hallock\*

*John A. Volpe National Transportation Systems Center  
Cambridge, MA 02142*

D. C. Burnham†

*Scientific and Engineering Solutions, Inc.  
Orleans, MA 02653*

## Abstract

For more than two decades cw doppler lidars have been used to study the decay of wake vortices generated by jet transport aircraft. With appropriate scan and data processing strategies, the vortex tangential velocity profile can be measured every few seconds. Under low turbulence conditions conducive to long vortex persistence the observed decay process is contrary to that predicted by classical theory and observed at low Reynolds numbers in wind tunnels and for small aircraft: namely, that the core grows in size and the maximum tangential velocity decreases while the total circulation remains roughly constant. For full-sized jet transport aircraft the vortex core often remains stable while the outer portion of the vortex decays, thereby reducing the total circulation. Data are presented from B-747 alleviation flight tests conducted in the 1970s and for other aircraft collected in the early 1990s. The stability of the core is consistent with the essentially laminar core flow observed via flow visualization.

## 1. Introduction

### 1.1 Lidar Wake Vortex Tests

The wake vortex data presented in this report were collected using a cw doppler lidar concept which was developed in the early 1970s. It was first deployed at Kennedy Airport to track and measure wake vortices<sup>1</sup>. The Kennedy tests were followed by a series of alleviation tests<sup>2,3</sup> designed to study how wake vortices could be alleviated by various flap and spoiler configurations for the Boeing-747. The Volpe Center was involved with the data analysis of the first alleviation test<sup>2</sup> and both data collection and analysis of subsequent tests. The data collection featured: (1) a scan strategy that gave good tangential velocity profiles and (2) a real-time display that permitted manual tracking of the vortices. The Volpe lidar was used to study rotorcraft wakes<sup>4</sup> in the mid 1980s. In 1990 it was used to study the wakes from the Boeing-727, -757 and -767 under unique desert conditions with mountain drainage flows<sup>5,6</sup> and in 1991, before its final

---

\*Manager Aviation Safety Division  
Senior Member AIAA

†President

retirement, it was deployed for a short test at the Dallas/Fort Worth Airport.

### 1.2 Scope of Paper

The alleviation test reports interpreted the results narrowly in terms of the immediate test goals. Subsequently, however, for those familiar with them, the results have revolutionized their understanding of the decay mechanisms for wake vortices from jet transport aircraft. In particular, the results indicate that the conventional decay mechanism of vortex core diffusion is not relevant to jet transport wakes. The purpose of this paper is to make this information and its interpretation available to all interested in wake vortex decay.

The data available for presentation in this paper are the published alleviation reports<sup>2,3</sup> and the data collected in the 1990s, which has not been reported in depth. The authors apologize for the quality of the figures from the alleviation reports which had to be scanned from hard copies, since neither the data nor the original figures are now available. Apologies are also in order for the mixture of English and metric units stemming from the long duration of the study.

This paper is declared a work of the U.S. Government and is not subject to copyright protection in the United States.

### 1.3 Vortex Profiles

After the wake roll-up process is complete, an aircraft wake can be described as two counter rotating, axially symmetric line vortices. Each vortex can be characterized by its tangential velocity profile  $v(r)$ , where  $r$  is the distance from the vortex center. The circulation profile  $\Gamma(r)$  can be calculated from the velocity profile:

$$\Gamma(r) = 2\pi r v(r). \quad (1)$$

As the vortex radius  $r$  increases, the circulation approaches an asymptotic value:

$$\Gamma(\infty) = W/K\rho Vb \quad (2)$$

where  $W$  = aircraft weight

$\rho$  = air density

$V$  = airspeed

$b$  = wingspan

$K$  = factor based on lift distribution ( $K = 1$  for uniform loading and  $K = \pi/4$  for elliptic loading).

### 1.4 Vortex Decay Mechanisms

The Greene model<sup>7</sup> of vortex decay indicates how turbulence and stratification affect the decay of total circulation (Equation 2) out of ground effect:

1. Turbulence has a direct effect on decay and causes the circulation to start decreasing immediately after wake generation.
2. The effect of stratification is related to buoyancy of the recirculation oval and is delayed since the buoyancy force is proportional to the distance the wake has descended.

The longest vortex lifetimes are expected when turbulence is low and atmospheric stratification is neutral. However, in practice low turbulence generally occurs only when the atmosphere is stratified (or perhaps for a short time after a stratified atmosphere becomes neutrally stratified). Cases with long-lived wake vortices were selected for this paper; consequently, the atmosphere was probably stratified for these cases. Note that, when wake vortices approach the ground, they are influenced by the additional effects of windshear and interaction with the surface boundary layer.

The vortex decay data presented in this paper are for wake vortices generated out of ground effect; however, the analysis will emphasize the detailed decay of the circulation profile (Equation 1), not the total circulation. Of course the two must be related; the profile decay data will provide some insight into the decay process.

Several aspects of this decay process are known qualitatively:

1. Flow visualization, whether from on-board or tower-mounted smoke sources, shows that, for large aircraft after vortex roll up, the flow in the vortex core *always* appears laminar with no turbulence. Even the complex roll-up processes that generate rotorcraft wake vortices<sup>4</sup> result in laminar cores.
2. The region outside the vortex core contains turbulence which comes from two sources: the aircraft and the atmosphere. Direct measurements of this turbulence can be made<sup>5</sup> with tower-mounted hot-wire anemometers.
3. Turbulence can cause decay of the outer vortex region via turbulent diffusion or, perhaps more importantly<sup>8</sup>, the distortion of turbulent eddies.
4. The edges of the vortex-pair recirculation oval may play an important role in vortex decay, particularly under stratified conditions. Sodars<sup>2</sup> observe enhanced turbulent scattering from the edge of the vortex oval under stratified conditions.
5. The Rayleigh instability dictates that the vortex circulation must increase with radius. Therefore, countersign vorticity wrapped around the outside of a vortex can effectively annihilate the outer vorticity of the vortex and force the circulation profile to be constant beyond a certain radius.

## 2. Lidar Characteristics

The lidar<sup>9</sup> is a cw backscatter homodyne system<sup>10</sup> operating at 10.6 microns with 20 W of transmitted power. Range resolution is achieved by focusing with a 30-cm diameter Cassegrain telescope; the focal range is adjusted by moving the secondary mirror. The range resolution (distance between half power points) is proportional to the range; since the measurements are poor when the resolution is either too large or too small, the useful operating range of the lidar is about 40 to 250 meters. The lidar response falls off slowly beyond the half power points and hence can respond to strong targets well outside the nominal range resolution. The backscatter signal is produced by atmospheric aerosols; smoke generators were mounted on the aircraft for the alleviation tests to provide flow visualization and to increase the lidar signal-to-noise ratio. The doppler shift in the scattered signal is a measure of the line-of-sight component of the atmospheric wind field. The beam scanner can vary the elevation angle from horizon to horizon. The lidar scans a plane perpendicular to the aircraft flight path by varying the range and elevation angle. Since the focal

spot is long in range and very narrow in angle, the most efficient scan method is to scan arcs in elevation at various fixed ranges.

The return signal is analyzed with a surface acoustic wave (SAW) spectrum analyzer that generates doppler spectra that are averaged for 2 or 4 msec. Since the range response is relatively broad, the resulting doppler spectrum contains contributions from different portions of the wake being measured. The largest doppler shift will come from the point where the lidar beam is tangent to the vortex tangential velocity. The return from this point will also give a peak in the spectrum since the line-of-sight velocity is constant for a distance along the beam approximately equal to the vortex radius. Thus, the lidar can measure the vortex tangential velocity even if it is not focused at the range to the vortex.

A human operator is required to track the wake vortices. A real-time display of the vortex tangential velocity is provided to show the operator where the vortices are located in the scan area, which typically consists of three to five ranges with an elevation angle sweep of up to 60 degrees. The operator adjusts the angle scan limits and the ranges to keep the vortices within the scan area.

The characteristics of the resulting vortex velocity profiles are shown in Figure 1, which shows data from three successive arc scans at different ranges for a DC-10 landing vortex at DFW airport (signal from natural aerosols). The vortex was located above the lidar (elevation angle of 107°), which minimizes the influence from:

1. The other vortex, and
2. The horizontal ambient wind.

The arc angles have been converted to distances from the vortex center. The vortex tangential velocity is assigned to the highest peak above a noise threshold in the doppler spectrum.

The two plots of Figure 1 can be understood as follows:

1. The upper plot shows the intensity of the peak above the noise threshold. The two lower ranges (410 and 336 feet) have comparable intensities which increase roughly linearly with vortex radius, as might be expected. The highest range (466 feet) has much lower peak intensities when the vortex peaks are above the detection threshold (vortex radius of 25 feet or greater). The observed intensities suggest that the actual vortex range is about midway between the second and third range (i.e., 373 feet).

2. The bottom plot shows the velocity bin of the peak; each bin corresponds to 0.55 m/s. The two sides of the vortex have opposite line-of-sight velocities but give the same sign doppler shift because the return signal is mixed with the transmitted signal. Where the peak intensities of the vortex tangential velocity peak are above the noise threshold (e.g., vortex radius above 25 feet for all ranges), all three arc scans give equivalent tangential velocities. Where the peak signal is below the noise threshold, the velocity drops below the actual tangential velocity. The velocity drop out at the vortex core is broad for the 466-foot range scan but much narrower for the other two scans which are much closer to the actual vortex range. For vortices with small cores and high core tangential velocities (typical for most of the jet transport fleet), the lidar cannot measure the core because of signal-to-noise-ratio limits.

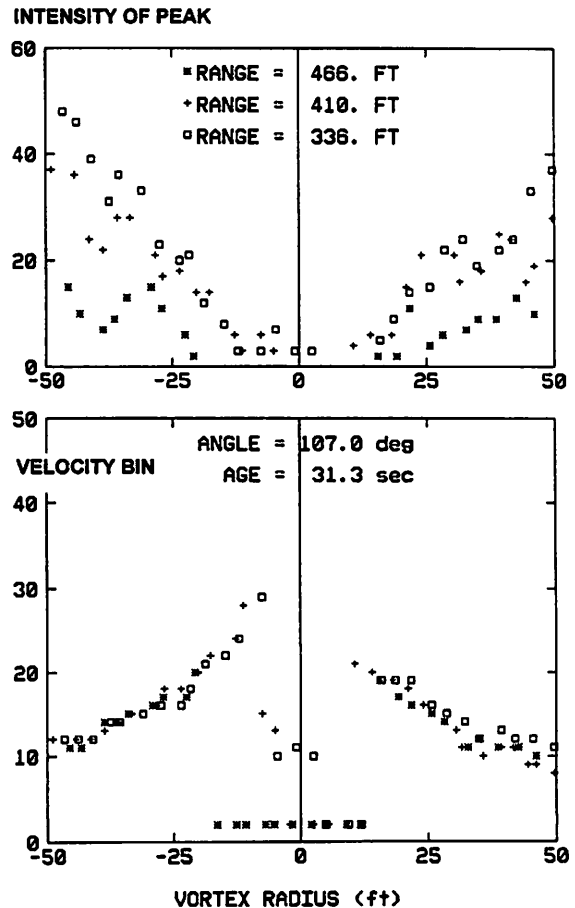


Figure 1. DC-10 Wake Vortex at DFW Airport: Highest Peak Algorithm for Three Arc Scans: Intensity and Velocity Bin

### 3. Alleviation Test Results

The alleviation tests<sup>2,3</sup> deployed spoilers during flight in order to reduce the strength of the vortex velocity flow field. Figure 2 shows<sup>2</sup> the effect of alleviation on the velocity profile of a B-747 in landing configuration; at an age of 24 seconds the roll-up processes are complete but little decay has occurred under the low turbulence conditions of the tests. The spoilers have reduced the maximum tangential velocity by almost a factor of two. The shape of the velocity profile is dramatically changed; the tangential velocity is constant from 1 to 12 meters. However, beyond 13 meters the velocity profile is essentially unchanged.

The alleviation tests included smoke generators at the wing tip and the outer edge of the outer flap. Since the final rolled up vortex core originates from one of these two locations (flap for normal landing configuration, wing-tip for alleviated landing configuration), the core had enhanced aerosol density. Because of the high scattered signal and relatively low core velocities, the core velocity profiles could often be resolved in the alleviation tests. Nevertheless, the core dropouts shown in Figure 1 were sometimes observed.

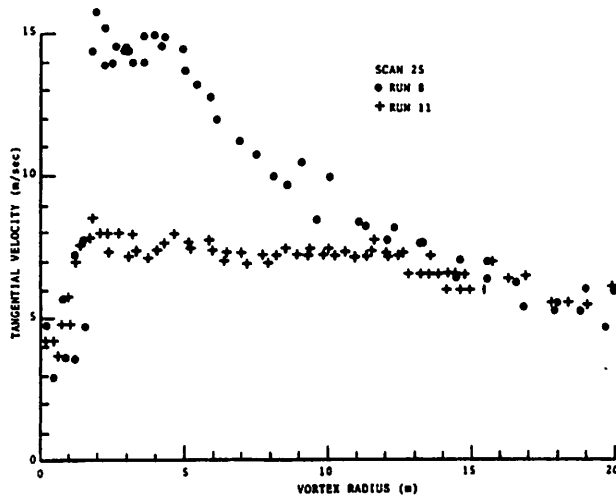


Figure 2. Comparison of Vortex Velocity Profiles at Age 24 seconds (Dot = Normal, Cross = Alleviated)

#### 3.1 First Alleviation Test

The first B-747 alleviation test<sup>2</sup> did not have the real-time tracking capabilities available for later tests. Fortunately two runs, one normal and one alleviated, were reasonably well tracked and were analyzed in detail. These runs (shown in Figure 2) gave the baseline B-747 circulation profiles used in subsequent data analysis.

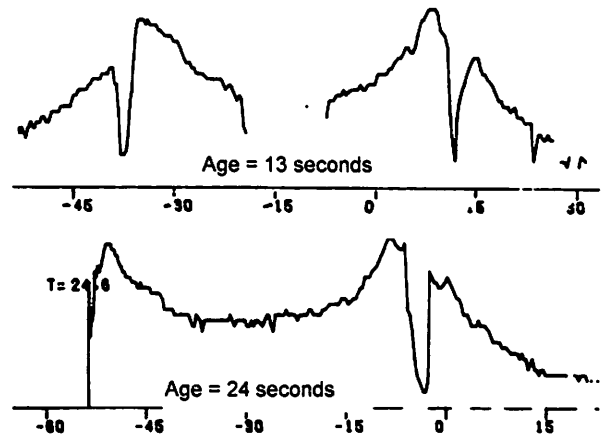


Figure 3. Tangential Velocity vs. Arc Distance (m) for Normal Run

Considerable processing was done to generate the data in Figure 2. Figure 3 shows the raw tangential velocity data for ages 13 and 24 seconds for the normal run shown in Figure 2; the lidar is looking up at the vortex pair. The velocity dips mark the locations of the vortex cores. The tangential velocity is actually negative between the two cores. Note that, at 13 seconds, the flow visualization gives clear velocity signals near the vortex cores but a dropout between the vortices. This dropout lasted until 24 seconds when the smoke had finally diffused to fill the region between the vortices. At 24 seconds the angle scan covered only half of the left vortex. Note that the smoke was more widely dispersed in the alleviated run; no dropout was noted between the two vortices.

The conversion of velocity profiles into circulation profiles via Equation 2 requires that the velocity asymmetry, caused by the line-of-sight motion of the vortex, be corrected so that the two sides of the vortex have equivalent circulation profiles. Figure 4 shows the circulation data for the two sides of the right vortex in the lower plot of Figure 3. The circulation data are well fitted with a straight line when the vortex radius is plotted on a logarithmic scale. The circulation for large radii is approximately equal to the 600 m<sup>2</sup>/s value expected for a B-747 according to Equation 2. Figure 5 shows similar plots for ages of 38, 54 and 75 seconds.

The straight line in Figures 4 and 5 is represented by the equation:

$$\Gamma(r) = \Gamma_c [1 + \ln(r/r_c)], \quad (3)$$

where  $\Gamma_c = 253 \text{ m}^2/\text{s}$  and  $r_c = 2.51 \text{ m}$ . The logarithmic form of this equation was proposed by Hoffman and Joubert<sup>11</sup> to describe turbulent vortices.

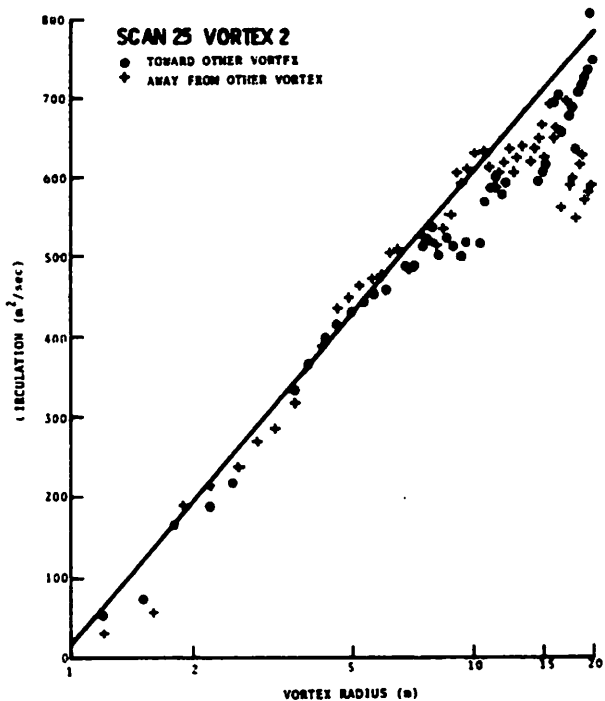


Figure 4. Circulation Profile for Normal Run at Age 24 seconds

The vortex decay observed in Figure 5 can be interpreted as follows:

1. The loss in circulation for radii below three meters in scans 39 and 55 is likely caused by the signal-to-noise core dropout illustrated in Figure 1.
2. The circulation for radii 4 to 6 meters remains reasonable well represented by Equation 3 until after scan 55. At scan 76 the circulation profile is represented by a parallel curve displaced downward by about 50 m<sup>2</sup>/s from the original curve.
3. The circulation beyond 6-meter radius decreases at

scan 55 and reaches a uniform value of about 400 m<sup>2</sup>/s at scan 76.

Figure 6 presents plots similar to those in Figures 4 and 5 for the alleviated run in Figure 2. In this case the vortex radius axis has a linear scale. Most plots have four sets of points, one for each vortex and one for each side of a vortex. The lines in the plots are given by the equation:

$$\Gamma(r) = \Gamma_c r / r_c \quad (4)$$

where  $\Gamma_c = 45 \text{ m}^2/\text{s}$  and  $r_c = 1.0 \text{ m}$ . Equation 4 is a good fit to the 24-second circulation profile.

The vortex decay in Figure 6 clearly starts at the outside and moves into smaller vortex radii, reaching a transition radius of 8 meters at 48 seconds and 4 meters at 81 seconds. Inside the transition radius the circulation changes very little in 81 seconds. Outside the transition radius the circulation is roughly constant and decreases to about 150 m<sup>2</sup>/s at 81 seconds.

### 3.2 Second Alleviation Test

The second B-747 alleviation test<sup>3</sup> consisted of four normal and seven alleviated out-of-ground-effect runs conducted on two separate days under low turbulence conditions (snow covered ground). The circulation profile decay plots (far too numerous to reproduce here) were essentially similar to those from the first alleviation test, although the vortex lifetimes were longer (perhaps because of improved vortex tracking).

Another plot format was used for these tests to display the entire run in a single plot. Figure 7 shows a normal run and Figure 8 an alleviated run, which immediately followed the normal run. These plots show the average circulation for both wake vortices. The average is calculated from zero radius up to four different radius values: 5, 10, 15 and 20 meters. Since the circulation increases with radius, the average

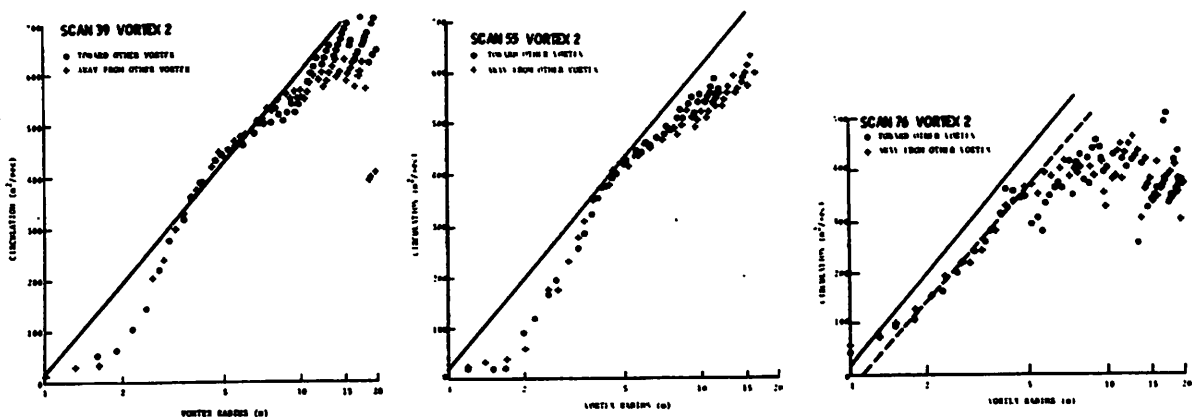


Figure 5. Circulation Profiles for Normal Run at Ages 39, 55 and 76 seconds

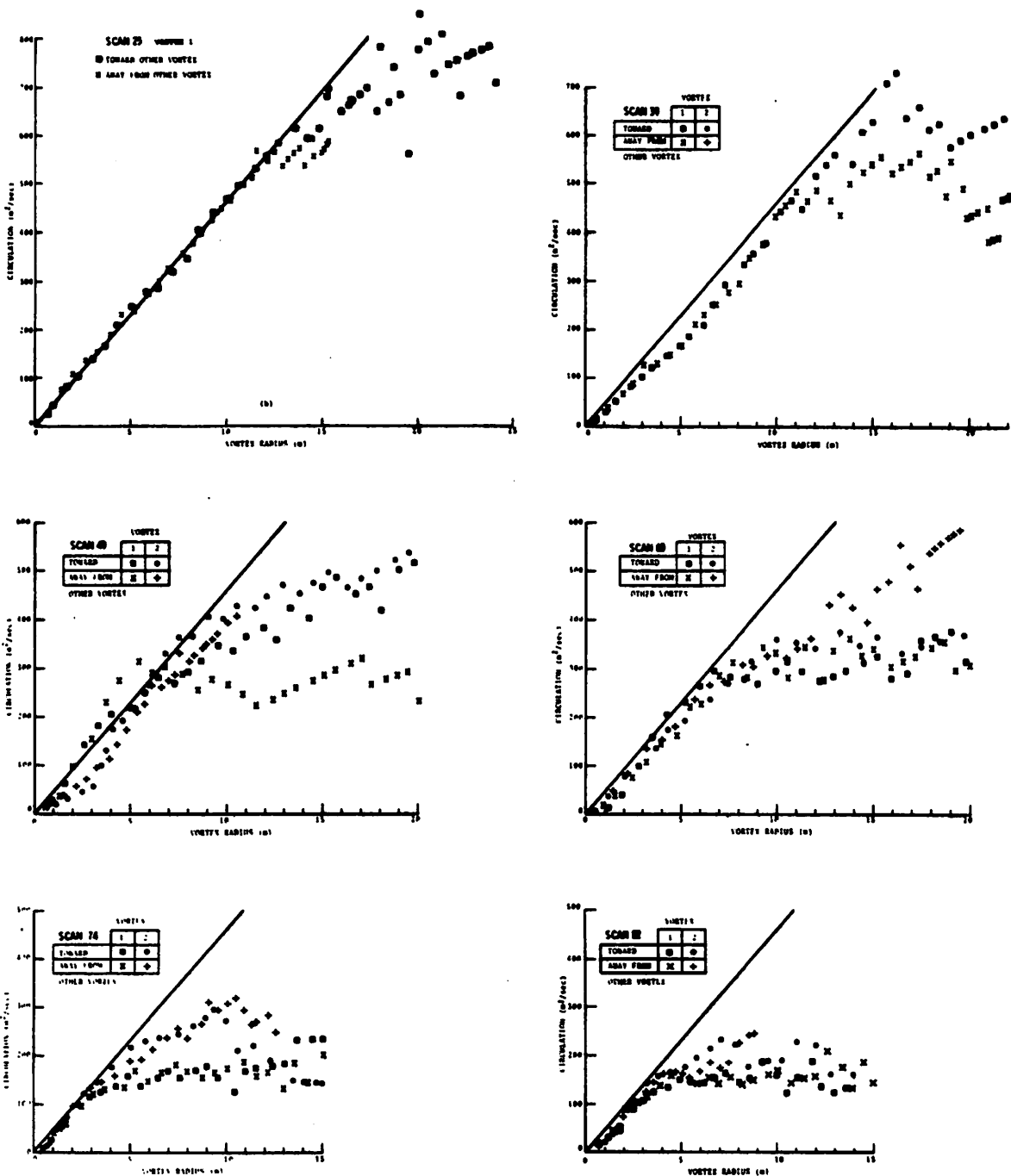


Figure 6. Circulation Profiles for Alleviated Run at Ages 24, 38, 48, 59, 73 and 81 seconds

circulation also increases as the radius is increased. The data point for each vortex averages over both sides of the vortex. The rationale for calculating average circulation is discussed in Section 5.3.

The roll up process for the normal run (Figure 7) leads to stable, consistent average circulation values by age 10 seconds. The 5-meter average circulation

(bottom line in Figure 7) remains constant until age 70 seconds before starting to decay. Thus, the vortex core remains unchanged for that time, just as noted in Figure 5. In contrast, the average circulation for larger averaging radii begin to decay immediately

The roll up process for the alleviated run (Figure 8) takes about 25 seconds to reach a stable

configuration (earlier times were omitted from Figure 6 for this reason). After that time the 5-meter average circulation remains constant until age 80 seconds before starting to decay. The average circulation for higher averaging radii starts to decay earlier at about 55 seconds.

### 3.3 Discussion

The circulation profile  $\Gamma(r)$  represents the integral of vorticity out to radius  $r$ . For the normal landing B-747 vortex half the vorticity is located within a radius of 3.5 meters and three quarters within a radius of 5.5 meters (see Figure 4). The alleviation process spreads out the vorticity so that half is located within a radius of a 6.5 meters and three quarters within a radius of 10 meters (see Figure 6, scan 25). The differences in the vorticity distribution for alleviated and normal vortices may permit the elucidation of different dissipative processes.

The decay of the circulation profile represents the diffusion of vorticity to larger radii. The vorticity in the core is locked up by the lack of turbulence and the ineffectiveness of normal viscous diffusion. This effect is noted in both normal and alleviated vortices. Outside the core, turbulent processes can transport vorticity to larger radii. This effect is more noticeable for normal than alleviated vortices. At larger radii vorticity can be canceled by countersign vorticity produced, for example, by buoyancy effects; the effect of this vorticity will propagate toward the vortex core via the Raleigh instability to give a circulation profile that is constant beyond a certain radius. This effect is more noticeable for alleviated than normal vortices. In Figure 6 the cancellation of vorticity clearly propagates in to smaller radii as time progresses. The same effect may be seen, but not so clearly, in Figure 8.

### 4. Recent Test Results

The 1990 and 1991 tests collected data from other types of aircraft than the B-747 used in the alleviation tests. The analysis methods used for the alleviation tests are not appropriate because the true core tangential velocities were never resolved (as in the core dropout in Figure 1). Consequently, recent studies<sup>6</sup> developed new analysis methods which did not require valid core measurements.

Since these tests were conducted relatively recently and utilized operator vortex tracking, the characteristics of vortex decay could be assessed in real-time. In particular, when a vortex decayed within the lidar scan area, the vortex signatures (see Figure 2) usually disappeared quickly, in five or ten seconds after the last good signature. The final vortex demise appears

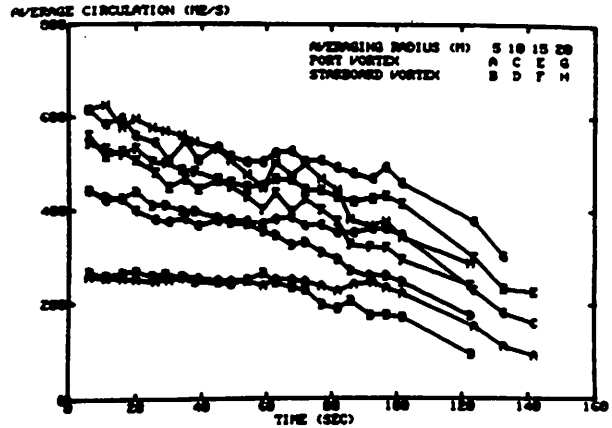


Figure 7. Decay of Average Circulation for Normal Run

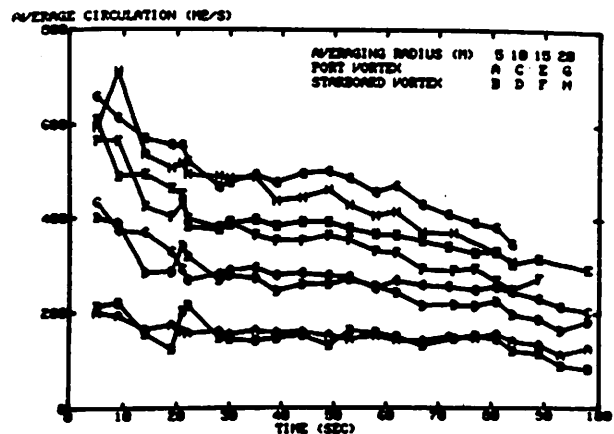


Figure 8. Decay of Average Circulation for Alleviated Run

to be a catastrophic event, perhaps related to the sinuous instability or vortex bursting.

### 4.1 Idaho Falls Test

Tower fly-by tests<sup>5</sup> are normally conducted with a crosswind that transports long-lived wake vortices out of lidar range before they decay. For two B-767 runs the crosswind was low enough that the upwind vortex could be tracked by the lidar operator until it disappeared. Note that these runs are not strictly out of ground effect and were not for landing configuration.

The decay of the circulation profile for these two runs is shown in Figures 9 and 10. The data in figure 9 lasts longer but starts at about 75 seconds. The data in Figure 10 start at about 25 seconds and therefore give a more complete picture of vortex decay. In this plot format the circulation profile is averaged over small increments of radius (5 feet) on both sides of the vortex and plotted against vortex age. In general, the circulation value increases with the averaging radii. The first increment, 0-5 feet, is omitted since it is completely inside the core velocity dropout (see Figure

1). The position of the core dropout for these runs was in the next increment, 5-10 feet, which is plotted but will have a value that depends upon the signal-to-noise-ratio. Therefore, the circulation values are valid only for increments greater than 5-10 feet. In fact, the increment 10-15 feet in Figure 10 shows the cleanest picture of vortex decay:

1. The circulation starts at about 70 percent of the total circulation and remains constant for about 60 seconds.
2. The circulation then decays more or less linearly to less than one third of the initial total circulation at age 160 seconds.

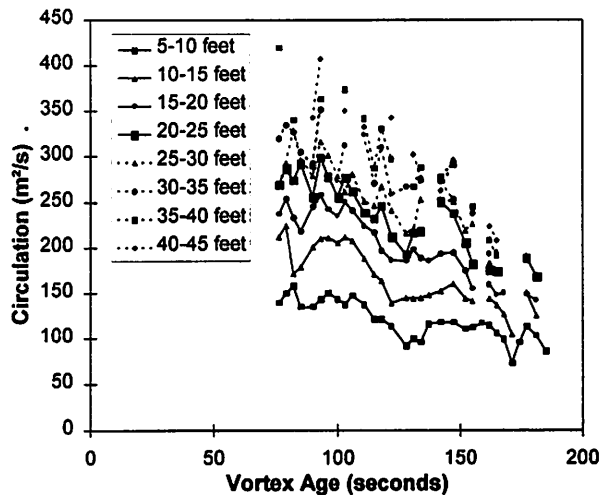


Figure 9. Circulation Profile Decay by Radius Increment for B-767 Run 10

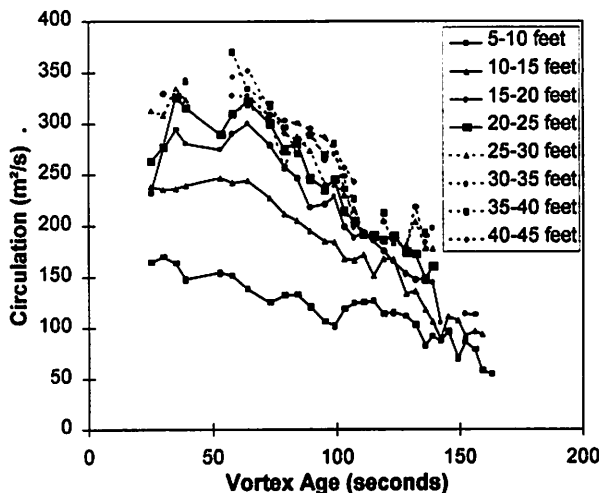


Figure 10. Circulation Profile Decay by Radius Increment for B-767 Run 23

The measured decay for higher increments in Figure 10 is more erratic. They show, however, that the outer portions of the vortex decay more rapidly than the 10-15-foot increment and reach comparable values at

vortex age 100 seconds. The 15-20-foot increment gives a reasonable estimate of the total circulation (as discussed in Section 5.3). The data in Figure 9 are noisier and do not permit such a clear interpretation. However, the 15-20-foot increment appears to give a plausible estimate of total circulation.

#### 4.2 Dallas/Fort Worth Airport

The lidar was installed under the approach path where the aircraft were at approximately 500-foot altitude. Vortices could be tracked until final demise only if the crosswind was low, which was not the case for most runs. Under heavy traffic conditions data could be collected only for every other arrival. The wake vortices from the previous run were still active when a new aircraft arrived. Of course, the normal vortex descent brought the old vortices well below the altitude of the new vortices, so that only one set could be selected for tracking.

A number of long-lived runs for different aircraft types were selected for analysis. Figures 11 through 14 are for the MD-80, B-737, B-727 and DC-10, respectively. All but the last tracked the vortex decay until the vortex signature disappeared.

The following observations can be made for these four runs:

1. The circulations for the four aircraft types are consistent with the sizes of the aircraft: smallest for MD-80 and B-737, larger for B-727 and even larger for DC-10.
2. The aircraft size also affects the validity of the various circulation profile increments. For example, the 5-10-foot increment appears to be mostly valid for the three smaller aircraft but not for the DC-10.
3. In all cases the 15-20-foot increments are plausible estimates for the total circulation.
4. Faster decay for the outer portion of the vortex is noted for the B-727 and possibly for the B-737 (but with a drop in core circulation between 40 and 50 seconds) but is not clearly seen for the MD-80 or DC-10. Additional cases of the DFW data set must be studied to obtain more definitive results.

### 5. Conclusions

#### 5.1 Vortex Decay Mechanism

The classical picture of vortex decay is viscous expansion of the core with constant total circulation. Although this picture describes the results of low Reynolds Number experiments, it is inconsistent with the high Reynolds Number data presented here for jet

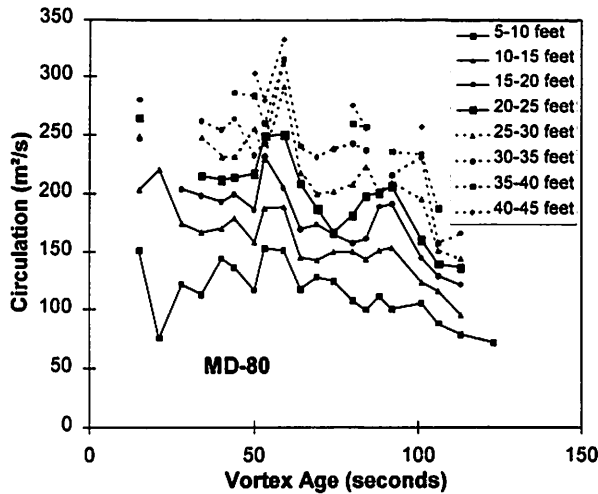


Figure 11. Circulation Profile Decay by Radius Increment for MD-80 Run

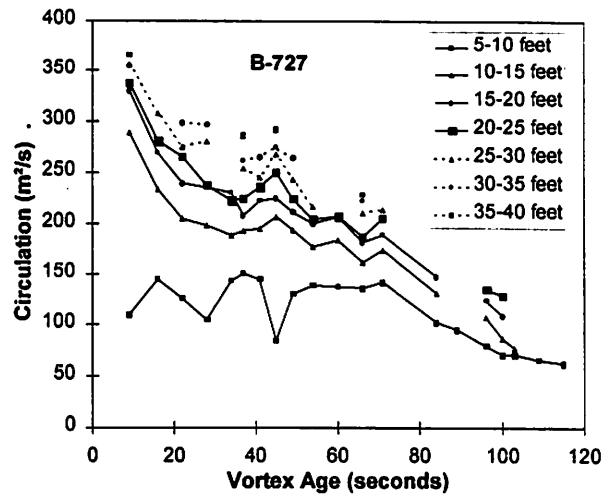


Figure 13. Circulation Profile Decay by Radius Increment for B-727 Run

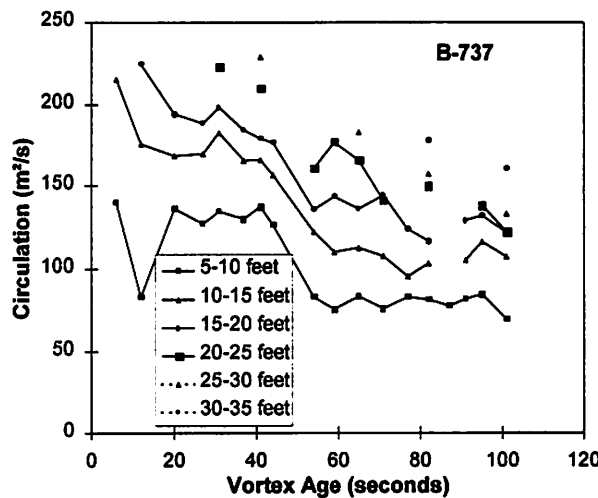


Figure 12. Circulation Profile Decay by Radius Increment for B-737 Run

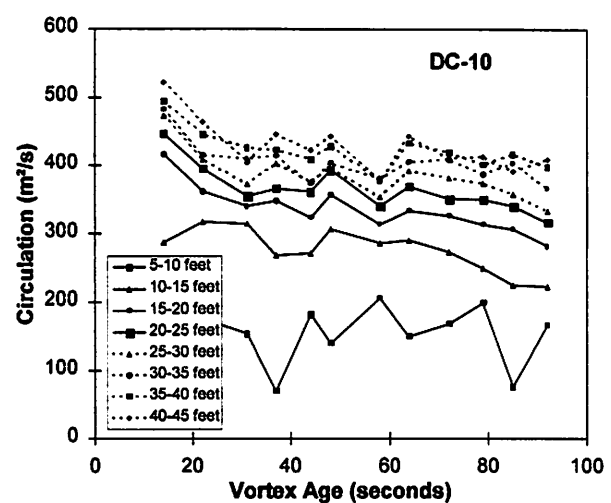


Figure 14. Circulation Profile Decay by Radius Increment for DC-10 Runs

transport aircraft. Note that the effects presented here for lidar data have also been noted in sodar measurements<sup>12</sup>. For such vortices the decay processes often affect the outer portion of the vortex rather than the core. Two processes could lead to this effect:

1. Countersign vorticity can be wrapped around the vortex by buoyancy forces, windshear gradient effects<sup>13</sup> or detachment of the ground boundary layer. The Rayleigh instability should cause this vorticity to effectively cancel the outer vorticity in the vortex.
2. Turbulence outside the vortex core can diffuse the vorticity out of the vortex or result in circulation decay via eddy distortion<sup>8</sup>.

The data set presented in this paper is limited in extent and contains no detailed consideration of meteorological conditions, which are known<sup>6</sup> to have a

major impact on vortex decay. The relationship of the decay mechanisms described in this paper to meteorological conditions should be addressed in future research.

## 5.2 B-747 Vortex Characteristics

The lidar velocity profiles presented in this paper for B-747 wake vortices are significantly different from those measured recently<sup>14</sup> at Heathrow airport. The latter show a smaller core with higher tangential velocities. In addition to this discrepancy, two other observations suggest that the wake vortices from the B-747 in landing configuration are unstable between two different vortex structures:

1. A vortex detection system based on acoustic refraction<sup>15</sup> is very sensitive to the vortex core size.

Vortex detection results were notably inconsistent for different B-747 arrivals.

2. The roll up of the B-747 wake, as viewed by flow visualization, was dramatically changed<sup>3</sup> by very small (only 7.5°) spoiler deflections. The vortex rolled up around the outer flap vortex with no spoilers and around the wing-tip vortex with spoilers deflected.

### 5.3 Vortex Strength Parameters

A number of parameters have been used to characterize vortex strength:

1. Total circulation,  $\Gamma(\infty)$ : can be calculated from aircraft and atmospheric parameters (Equation 1) but is difficult to measure directly because the tangential velocity becomes comparable to the velocity measurement error at large vortex radii.
2. Average circulation,  $\Gamma(a,c)$ , from radius  $a$  to radius  $c$ : The average circulation with  $a=0$  is approximately proportional to the rolling moment induced on a wing of span  $b=2c$  centered in the vortex flow field. While this parameter can be used to estimate the impact of a wake vortex encounter, it suffers from its sensitivity to the capability of a vortex sensor to measure the vortex core velocities. For example, sodar and lidar average circulation measurements of the same vortex can have dramatically different values<sup>16</sup> because of the lower spatial resolution and core anomalies of the sodar.
3. The maximum tangential velocity has been used<sup>17</sup> to characterize the vortex strength. This parameter is difficult to measure for small vortex cores and has *no known relationship* to the hazard of a wake vortex encounter.

The observation presented in this paper [that the vortex circulation profile often decays to a form where the circulation is approximately constant outside the vortex core] suggests that the average circulation with radius  $a$  outside the core will give a reasonable estimate of total circulation for decayed vortices. If the range from  $a$  to  $c$  is selected to exclude invalid or noisy data for a particular sensor, then the resulting circulation estimate should be independent of the measurement method.

### Acknowledgments

This work was sponsored by the Federal Aviation Administration. The authors would like to thank George Greene for helpful discussions.

### References

- <sup>1</sup> Bilbro, J.W. et al 1976: "Laser Doppler Velocimeter Wake Vortex Tests," NASA Tech Memo No. X-64988, March 1976.
- <sup>2</sup> Burnham, D.C. et al 1978: "Ground-Based Measurements of the Wake Vortex Characteristics of a B-747 Aircraft in Various Configurations," DOT Report No. FAA-RD-78-146, December 1978.
- <sup>3</sup> Burnham, D.C. 1982: "B-747 Vortex Alleviation Flight Tests: Ground-Based Sensor Measurements," DOT Report No. DOT-FAA-RD-81-99
- <sup>4</sup> Teager, S.A. et al 1996: "Flight Test Investigation of Rotorcraft Wake Vortices in Forward Flight," DOT Report No. DOT/FAA/CT-94/117, February 1996.
- <sup>5</sup> Page, R.D. et al 1992: "Panel Discussion on Tower Fly-By Testing 1990 Fall Series," Proceedings of the Aircraft Wake Vortices Conference, DOT Report No. DOT/FAA/SD-92/1.2, June 1992, pp. 49-(1-53).
- <sup>6</sup> Rudis, R, Burnham, D. and Janota, P. 1996: "Wake Vortex Decay near the Ground under Conditions of Strong Stratification and Wind Shear," AGARD-CP-584 Conference Proceedings The Characterisation & Modification of Wakes from Lifting Vehicles in Fluids, 20-23 May 1996, Trondheim, Norway, November 1996, pp. 11-(1-10).
- <sup>7</sup> Greene, G.C. 1986: "An Approximate Model of Vortex Decay in the Atmosphere," *J. Aircraft*, Vol. 23, July 1986, pp. 566-573.
- <sup>8</sup> Corjon, A., Risso, F., Stoessel, A., and Poinot, T. 1996: "Three Dimensional Direct Numerical Simulations of Wake Vortices: Atmospheric Turbulence Effects and Rebound with Crosswind," AGARD-CP-584 Conference Proceedings The Characterisation & Modification of Wakes from Lifting Vehicles in Fluids, 20-23 May 1996, Trondheim, Norway, November 1996, pp. 28-(1-21).
- <sup>9</sup> Brashears, M.R., Lawrance, T.R. and Zalay, A.D. 1977: "Mobile Laser Doppler System Checkout and Calibration," DOT Report FAA-RD-77-48, June 1977.
- <sup>10</sup> Sonnenschein, C.M. and Horrigan, F.A. 1971: "Signal to Noise Relationships for Coaxial Systems that Heterodyne Backscatter from the Atmosphere," *Applied Optics*, Vol. 10, No. 7, July 1971, pp. 1600-1604.
- <sup>11</sup> Hoffman, E.R. and Joubert, P.N. 1963: "Turbulent Line Vortices," *J. Fluid Mech.*, Vol. 16, Part 3, July 1963, pp. 395-411.
- <sup>12</sup> Sullivan, T. et al 1979: "Aircraft Wake Vortex Takeoff Tests at Toronto International Airport," DOT Report No. FAA-RD-78-143, February 1979, p. 7-49.

---

<sup>13</sup> Burnham, D.C. 1972: "Effect of Ground Wind Shear on Aircraft Trailing Vortices," *J. Aircraft*, Vol. 10, No. 8, August 1972, pp. 1114-1115.

<sup>14</sup> Vaughan, J.M. et al 1996: "Structure, Trajectory and Strength of B747 Aircraft Wake Vortices Measured by Laser," AGARD-CP-584 Conference Proceedings The Characterisation & Modification of Wakes from Lifting Vehicles in Fluids, 20-23 May 1996, Trondheim, Norway, November 1996, pp.10-(1-10).

<sup>15</sup> Burnham, D.C. 1977: "Characteristics of a Wake-Vortex Tracking System Based on Acoustic Refractive Scattering," *J. Acoustical Soc. America*, Vol. 61, March 1977, pp. 647-654.

<sup>16</sup> Rudis, R.P. and Burnham, D.C. 1996: "Comparison of Sodar and Lidar Measurements of Aircraft Wake Vortices," Preprint for ISARS'96 Conference, Moscow, Russia, May 1996.

<sup>17</sup> Garodz, L.J. and Clawson, K.L. 1993: "Vortex Wake Characteristics of B757-200 and B767-200 Aircraft Using the Tower Fly-By Technique," NOAA Tech Memo ERL ARL-199, January 1993.